Supplementary information for

Dynamics of China's Forest Carbon Storage: The First 30 m Annual Aboveground Biomass Mapping from 1985 to 2023

Yaotong Cai [a], Peng Zhu [b], Xing Li [a], Yuhe Chen [a], Qianhui Shen [a], Xiaocong Xu [a], Honghui Zhang [c], Sheng Nie [d, e], Cheng Wang [d, e], Jia Wang [f, g], Bingjie Li [a], Changjiang Wu [a], Haoming Zhuang [a*], Xiaoping Liu [a*]

[a] *School of Geography and Planning, Sun Yat-Sen University, Guangzhou 510275, China*

[b] *Department of Geography, The University of Hong Kong, Hong Kong SAR 999077, China*

[c] *Guangdong Engineering Center for Intelligent Spatial Planning, Guangdong Guodi Planning Science Technology Co. Ltd, Guangzhou, 510650, China*

[d] *International Research Center of Big Data for Sustainable Development Goals, Beijing 100094, China*

[e] *Key Laboratory of Digital Earth Science, Aerospace Information Research Institute, Chinese Academy of Sciences, Beijing 100094, China*

[f] *Beijing Key Laboratory of Precision Forestry, Beijing Forestry University, Beijing, 100094, China*

[g] *Ministry of Education of Engineering Research Center for Forest and Grassland Carbon Sequestration, Beijing Forestry University, Beijing, 100094, China*

* Address correspondence to: liuxp3@mail.sysu.edu.cn (X. Liu)

The supplementary materials include:

Supporting Text S1–S5

Tables S1–S2

Figures S1–S4

Bibliography

Text S1–S5

Text S1 | Overviews of the study area

Spanning a vast land area of 9.6 million square kilometers, China encompasses diverse landscapes and five major climate zones: cold temperate, temperate, warm temperate, subtropical, and tropical. Nationally, the land area comprises 33.3% mountains, 26% plateaus, 18.8% basins, 12% plains, and 9.9% hills. According to the Ninth National Forest Inventory (NFI), natural forests account for 63.55% of the total forest area in China, while planted forests cover 36.45%. Of these planted forests, 72.88% consist of young and middle-aged stands, resulting in a lower average AGBD of 59.25 Mg/ha compared to 112.21 Mg/ha for natural forests (National Forestry and Grassland Administration, 2019). Natural forests are primarily distributed in the northeastern, southwestern, and northwestern regions, which are also key hotspots for forest AGB. Planted forests, on the other hand, are mainly distributed in the central, southern, and eastern regions. In the northeast, boreal forests and mixed conifer-broadleaf forests dominate, with key species including Larix spp. and Abies spp. In the southwest, high-altitude conifer forests and mixed conifer-broadleaf forests are prevalent, with species such as *Picea* spp., *Abies* spp., and broadleaf species like *Quercus* spp. and *Acer* spp. The northwest region features arid and semi-arid forests interspersed with desert and steppe ecosystems, with drought-resistant species like *Haloxylon* spp. and *Populus euphratica.* In northern China, temperate deciduous broadleaf forests and forests of *Pinus tabuliformis* and *Platycladus orientalis* (Chinese arborvitae) are found. In central China, forests are primarily temperate deciduous broadleaf forests, thriving in hilly and basin landscapes, with species like *Robinia pseudoacacia* (black locust) and *Fraxinus* spp. (ash). In the southern regions, there are *Pinus massoniana* (Masson pine) and *Cunninghamia lanceolata* (China fir) forests, evergreen broadleaf forests, and economic forests such as *Camellia* spp., *Vernicia fordii* (tung oil tree), and other species.

Text S2 | AGB Datasets for comparison

AGB datasets utilized for spatial comparison

For the spatial comparison of forest AGB, we utilized six external AGB datasets with different spatial resolutions and temporal coverage. These datasets provide global and national-scale AGB estimates, enabling us to assess the spatial consistency of our AGB model. An overview of these datasets is provided in Text Table 1.

1. **Zarin Map** (2000, Global, 30 m): This dataset provides a global AGB map based on field measurements and remote sensing data. It offers high spatial resolution (30 m) and was created by Zarin et al. (2016) for global AGB estimation.

2. **Hu Map** (2004, China, 1000 m): Hu et al. (2016) developed this dataset specifically for China, providing AGB estimates at a spatial resolution of 1000 meters. It is based on remote sensing data and field measurements and is useful for comparing AGB estimates across large-scale areas in China.

3. **Su Map** (2004, China, 1000 m): Another dataset for China, created by Su et al. (2016) with the same spatial resolution as the Hu map (1000 m). It uses similar methods to the Hu map but incorporates different field data, making it valuable for cross-validating AGB estimates at national scales.

4. **Santoro Map** (2010, Global, 100 m): The Santoro et al. (2021) dataset provides global AGB estimates at a 100-meter resolution. This map was generated using a combination of field data and remote sensing inputs, and it is important for evaluating the global spatial patterns of AGB.

5. **Yang Map** (2019, China, 30 m): Yang et al. (2023) developed this dataset for China with a high spatial resolution of 30 meters. It offers valuable insights into more recent AGB conditions in China, serving as a useful comparison for our own AGB estimations.

6. **ESA CCI** (2010, 2017–2020, Global, 100 m): The European Space Agency's Climate Change Initiative (ESA CCI) AGB dataset provides global AGB estimates at a resolution of 100 meters for multiple years. The dataset, covering 2010 and 2017-2020, is useful for comparing spatial variations in AGB across different biomes.

These datasets cover various regions and resolutions, and by comparing them with our model's AGB estimates, we can assess both the consistency and accuracy of our spatial predictions.

Text Table 1. Overview of external AGB datasets utilized for spatial comparison.

Dataset	Regions	Temporal scope	Spatial resolution	Sources
Zarin map	Global	2000	30 m	Zarin et al., (2016)
Hu map	China	2004	1000 m	Hu et al., (2016)
Su map	China	2004	1000 m	Su et al., (2016)
Santoro map	Global	2010	100 m	Santoro et al., (2021)
Yang map	China	2019	30 m	Yang et al., (2023)
ESA CCI	Global	2010, 2017–2020	100 m	Santoro et al., (2023)

AGB datasets utilized for dynamic comparison

In addition to spatial comparisons, we also evaluated the dynamic changes in AGB across time using four external datasets. These datasets cover different temporal periods and provide valuable insights into the temporal dynamics of forest biomass. The details of these datasets are summarized in Text Table 2.

1. **Liu Map** (1993–2012, Global, 0.25°): Liu et al. (2015) developed this dataset, which provides annual AGB estimates at a spatial resolution of 0.25°. Spanning nearly two decades, it allows for the examination of long-term trends in global AGB and serves as a basis for comparing dynamic changes in forest biomass.

2. **Hengeveld Map** (1950–2010, Global, 1°): The Hengeveld et al. (2015) dataset offers AGB estimates at 1° spatial resolution at five-year intervals from 1950 to 2010. It provides a historical perspective on global AGB changes and is valuable for understanding long-term biomass trends, especially in regions with limited recent data.

3. **Chen Map** (2002–2021, China, 1000 m): This dataset, developed by Chen et al. (2023), provides annual AGB estimates at 1000-meter resolution for China. Spanning nearly two decades, it offers insights into the dynamics of forest biomass in China, which is crucial for evaluating the performance of our AGB model over time in this region.

4. **ESA CCI** (2010, 2017–2020, Global, 100 m): Similar to its use in spatial comparisons, the ESA CCI AGB dataset also provides temporal information, offering AGB estimates for 2010 and 2017-2020. With a 100-meter resolution, this dataset allows for examining recent changes in AGB at the global scale, complementing the dynamic comparison of biomass changes.

These datasets enable a comprehensive evaluation of dynamic changes in forest AGB over time. By comparing the temporal trends observed in these datasets with our model's predictions, we can assess how well our model captures AGB dynamics and how it performs in comparison to other established AGB products.

Text Table 2. Overview of external AGB datasets utilized for dynamic comparison.

Dataset	Regions	Temporal scope	Spatial resolution	Sources
Liu map	Global	1993–2012 (Annual)	0.25°	Liu et al., (2015)
Hengeveld map	Global	1950–2010 (5 years intervals)	1°	HENGEVELD et al., (2015)
Chen map	China	2002–2021 (Annual)	1000 m	Chen et al., (2023)
ESA CCI	Global	2010, 2017–2020	100 m	Santoro et al., (2023)

Text S3 | Model comparison

We compared the performance of three machine learning models—Random Forest, XGBoost (Extreme Gradient Boosting), and LightGBM (Light Gradient Boosting Machine)—with the ResNet model, which was developed for forest AGBD estimation.

Random Forest

RF is an ensemble learning method that builds multiple decision trees during training and combines their predictions to improve accuracy and reduce overfitting (Breiman, 2001). Each tree in the forest is trained on a bootstrap sample of the dataset, and a random subset of features is considered for splitting at each node, which increases model robustness and reduces the likelihood of overfitting. RF is particularly effective for high-dimensional datasets and is capable of handling both regression and classification tasks. The output for regression tasks is the average prediction across all trees, providing a stable and reliable result. Key advantages include its ability to capture nonlinear relationships and its robustness to noise, but its interpretability is limited due to the ensemble structure.

XGBoost

XGBoost is a scalable and efficient gradient boosting framework designed for both classification and regression tasks (Chen et al., 2016). It employs a sequential ensemble of decision trees, where each tree is trained to correct the residual errors of its predecessors, optimizing a specified loss function. Key features of XGBoost include regularization techniques (L1 and L2) to prevent overfitting, tree pruning based on a minimum loss reduction threshold, and support for sparse data handling. It also incorporates parallel processing, making it computationally efficient and suitable for large datasets. XGBoost's flexibility and strong predictive performance have made it one of the most widely used machine learning methods in competitions and applications.

LightGBM

LightGBM is a gradient boosting framework specifically designed for speed and efficiency on large datasets (Ke et al., 2017). Unlike traditional boosting methods, LightGBM uses a histogram-based algorithm and a leaf-wise tree growth strategy with depth constraints. This approach significantly reduces computational cost and memory usage while improving accuracy. It supports categorical feature handling, parallel learning, and distributed training. LightGBM is particularly

effective for tasks with large-scale data and high dimensionality, achieving faster training times compared to XGBoost while maintaining comparable or superior performance. However, it may require careful tuning of hyperparameters to avoid overfitting.

Parameters setting

Each model was trained using the same set of input features, including Landsat spectral bands, vegetation indices, and additional auxiliary variables such as climatic factors (mean annual temperature and precipitation), topographic features (elevation, slope, and aspect), geolocation (latitude and longitude), and tree cover. For RF model, we set the number of trees to 500, with a maximum depth of 30 for each tree and the minimum samples per leaf set to 1 to ensure model flexibility. For XGBoost model, the learning rate was set to 0.05, with 1000 boosting rounds and a maximum depth of 6 for each tree. The model also used L2 regularization to prevent overfitting. For LightGBM model, we used 1000 boosting iterations with a learning rate of 0.05, and the maximum depth of trees was set to 6. Additionally, we used the "dart" boosting type for enhanced model robustness. We evaluated the accuracy and predictive performance of each model across five AGBD intervals: 0–50, 50–100, 100–150, 150–200, and ≥200 Mg/ha. This interval-based analysis enabled us to assess model performance under varying biomass conditions, particularly addressing the spectral saturation issue often observed in higher AGBD ranges when using only multispectral data.

ResNet outperforms ML ensemble models

All three traditional machine learning algorithms achieve good fitting accuracy, with Random Forest performing the best (R^2 = 0.90), followed by XGBoost (R^2 = 0.83) and LightGBM (R^2 = 0.74). Although the fitting accuracy of Random Forest is comparable to that of ResNet (R^2 = 0.92, RMSE = 16.01 Mg/ha), it is more prone to the effects of spectral saturation, particularly in high-biomass areas (Text Table 3). In regions where biomass exceeds 150 Mg/ha, traditional machine learning models tend to underestimate AGBD, with the degree of underestimation increasing as forest biomass rises.

In contrast, deep learning models, such as ResNet, do not exhibit significant underestimation; AGBD predictions remain distributed around the 1:1 line in scatter plots (Text Fig. S1a). Notably, in areas where forest AGBD exceeds 200 Mg/ha, the systematic bias from ResNet underestimation (-24.63 Mg/ha) is considerably lower than that of the other three models (Random Forest: -54.19

7

Mg/ha; XGBoost: -67.02 Mg/ha; LightGBM: -90.84 Mg/ha) (Text Table 3). This suggests that deep learning methods can better capture the complex relationship between biomass and spectral features, effectively reducing the impact of spectral saturation on AGBD estimation compared to traditional machine learning models.
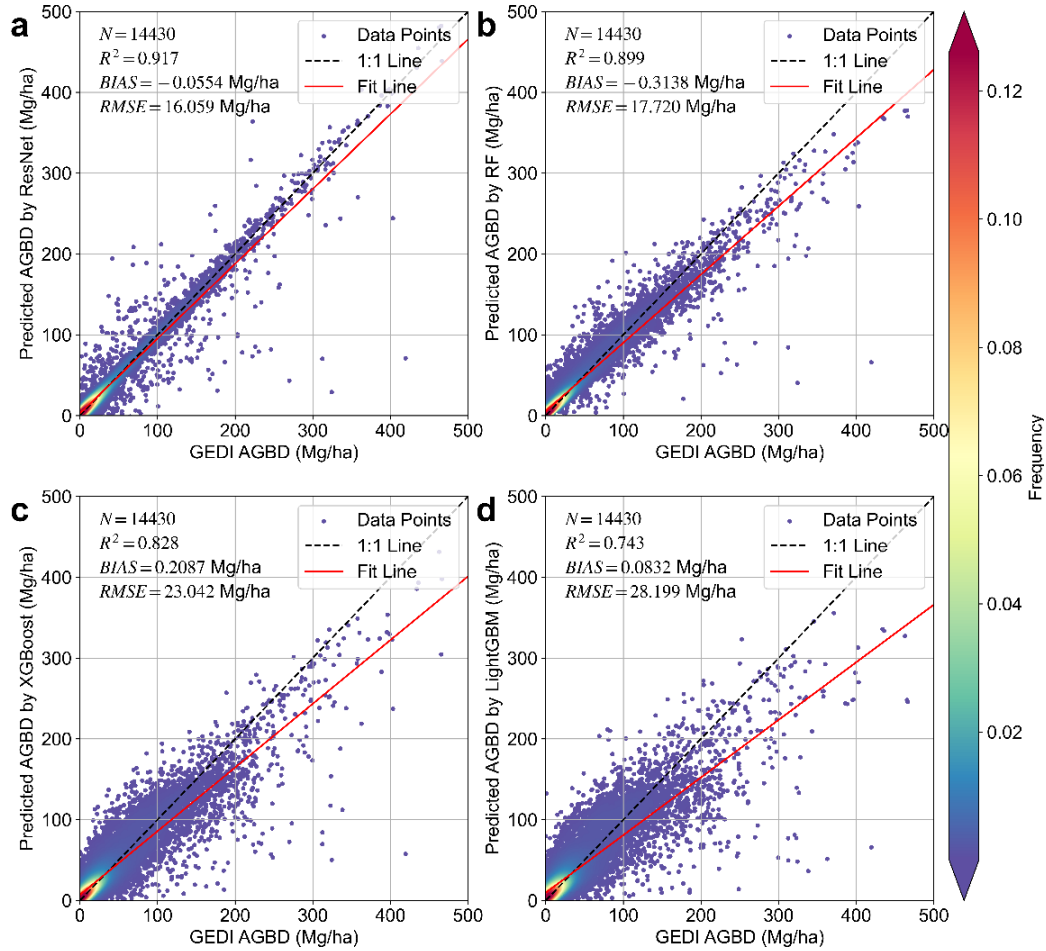
Text Fig. S1 | Comparison of AGBD estimation accuracy using different algorithms. (a) Scatter plot of GEDI AGBD vs. ResNet estimated AGBD. (b) Scatter plot of GEDI AGBD vs. Random Forest estimated AGBD. (c) Scatter plot of GEDI AGBD vs. XGBoost estimated AGBD. (d) Scatter plot of GEDI AGBD vs. LightGBM estimated AGBD.

Text Table 3. Estimation accuracy of different models along AGBD intervals.

Intervals of AGBD (Mg/ha)	Models	RMSE (Mg/ha)	Bias (Mg/ha)
[0, 50)	ResNet	7.79	1.26
	RF	7.96	2.40

	XGBoost	11.64	3.44
	LightGBM	12.72	4.18
[50, 100)	ResNet	17.41	-0.34
	RF	19.23	2.76
	XGBoost	27.75	0.34
	LightGBM	31.03	2.58
[100, 150)	ResNet	20.35	-2.94
	RF	20.98	-3.97
	XGBoost	31.66	-10.96
	LightGBM	34.69	-11.71
[150, 200)	ResNet	28.56	-6.91
	RF	30.70	-18.25
	XGBoost	48.10	-32.50
	LightGBM	56.34	-38.33
≥200	ResNet	78.17	-24.63
	RF	89.83	-54.19
	XGBoost	101.08	-67.02
	LightGBM	137.84	-90.84

Text S4 | Forest carbon sink over China

Our findings are consistent with previous studies, confirming that China's forests have served as a significant carbon sink over the past few decades. We estimate that China's forests absorbed an average of 0.21 ± 0.04 PgC per year from 1985 to 2023. This falls within the range reported by earlier studies based on forest inventories, satellite observations, atmospheric inversions, and process-based models, which estimate forest carbon sinks ranging from 0.18 to 0.45 PgC per year (Yu et al., 2022). Our result is slightly higher than Piao et al., (2009), who estimated an average of 0.17 PgC per year for the period 1980–2002, and Fang et al., (2024), who reported 0.16 PgC per year for forest AGC changes between 2015 and 2021. Similarly, He et al., (2019) used three process-based models to estimate a carbon sink of 0.12 PgC per year for China's terrestrial ecosystems from 1982 to 2010. Comparatively, Zhao et al., (2021) estimated a forest carbon sink of 0.102 PgC per year for 1997–2018 using MODIS satellite and forest inventory data, while Harris et al., (2021) reported an average of 0.14 PgC per year for 2000–2019. Pan et al., (2011) similarly found a lower carbon sink of 0.115 PgC per year for the period 2000–2007. However, our results are significantly higher—approximately 3.5 times larger—than those of Yin et al., (2015), who used machine learning methods to estimate forest aboveground carbon stock changes at 0.062 PgC per year for 2001–2013, and more than double the estimate by Chen et al., (2023), who reported 0.062 PgC per year for 2000–2021.

The differences in these estimates likely arise from variations in forest area estimates, as forest expansion has been a primary driver of changes in China's landscape and terrestrial carbon sink since 1980 (Cai et al., 2024; Xia et al., 2023; Yu et al., 2022). Our study, which leverages the China Annual Terrestrial Carbon Dynamics Dataset (CATCD)—the first high spatiotemporal resolution remote sensing product to fully reconstruct China's forest area expansion over the past 40 years—produces results closely matching those of Yu et al., (2022). Their study, using the Dynamic Land Ecosystem Model (DLEM), reported a forest carbon sink of 0.21 ± 0.006 PgC per year from 1980 to 2019. This is likely because Yu et al., (2022) also corrected biases in historical forest area data caused by inconsistent reporting methodologies.

Additionally, Wang et al., (2020) demonstrated that bottom-up approaches might substantially underestimate China's terrestrial carbon sink, with atmospheric CO_2 data indicating an average

carbon uptake of -1.11 ± 0.38 PgC per year for 2010–2016. This highlights the importance of developing a comprehensive understanding of carbon dynamics in China's forests. Future research is needed to reconcile discrepancies across methods and datasets to achieve a more accurate understanding of China's forest carbon dynamics.

Text S5| Integrating Sentinel-1 for AGB estimation

Estimating forest AGB using optical imagery often encounters challenges due to spectral saturation, wherein the spectral signals captured by optical sensors exhibit limited variability as forest biomass reaches certain levels. This saturation effect compromises the optical imagery's ability to distinguish between different biomass levels, particularly in regions with high biomass density. To evaluate the feasibility of estimating forest AGBD using multispectral imagery and assess the benefits of integrating Sentinel-1 SAR data in reducing saturation issues, we employed two modeling strategies: (1) the Multispectral-Only Model, which used Landsat-derived spectral bands and vegetation indices as explanatory variables, and (2) the Multispectral + SAR Model, which incorporated Sentinel-1 VV and VH backscatter coefficients in addition to the same variables used in the first model. Both models also included auxiliary features, such as climatic variables (mean annual temperature and precipitation), topographic factors (elevation, slope, and aspect), geolocation information (latitude and longitude), and tree cover (see Fig. 2). These features were derived from external datasets and resampled to match the spatial resolution and extent of the Landsat composites. To assess model performance under varying biomass conditions, we divided the AGBD estimates into five intervals based on 50 Mg/ha increments: 0–50, 50–100, 100–150, 150–200, and ≥200 Mg/ha. For each interval, we calculated the root mean squared error (RMSE) and bias for both modeling strategies, focusing on the spectral saturation issue typically observed in higher AGBD ranges when using only multispectral data.

Sentinel-1 data and preprocessing

Sentinel-1, part of the European Space Agency's (ESA) Copernicus Earth Observation Programme, is a synthetic aperture radar (SAR) mission designed for all-weather, day-and-night Earth observation at C-band. The mission employs two satellites, Sentinel-1A and Sentinel-1B, with a revisit time of 6–12 days and a native spatial resolution of 10 meters. Sentinel-1 operates in multiple acquisition modes, and this study utilizes data from the Interferometric Wide Swath (IW) mode, which is optimized for land monitoring. We accessed Sentinel-1 Ground Range Detected (GRD) scenes via the Google Earth Engine (GEE) platform. Preprocessing included radiometric calibration, terrain correction, and resampling to 30-meter resolution to match the spatial scale of Landsat composites. To align with the growing season used in Landsat processing (day of year 150–

270), we selected Sentinel-1 GRD scenes within this period and generated annual median composites based on VV (vertical transmit and vertical receive) and VH (vertical transmit and horizontal receive) polarization backscatter coefficients.

Sentinel-1 Enhances AGBD Estimates

Our findings indicate that the model incorporating SAR features outperforms the base model (Text Table 4). Particularly in cases where AGBD exceeds 150 Mg/ha, the inclusion of SAR features effectively mitigates the challenges posed by spectral saturation. Despite the performance enhancement, the two models produce highly correlated AGBD predictions, as indicated by a correlation coefficient of r=0.96 (p<0.0001) (Text Fig. S2). This implies that while leveraging SAR data provides benefits, estimating AGBD solely based on spectral features remains a feasible approach, especially in historical years lacking SAR data availability. Integrating SAR features into AGBD estimation models offers a promising avenue for improving accuracy, particularly in regions where optical imagery alone may face limitations. Nonetheless, the continued viability of spectral-based AGBD estimation underscores the importance of considering practical constraints and data availability when selecting modelling approaches.
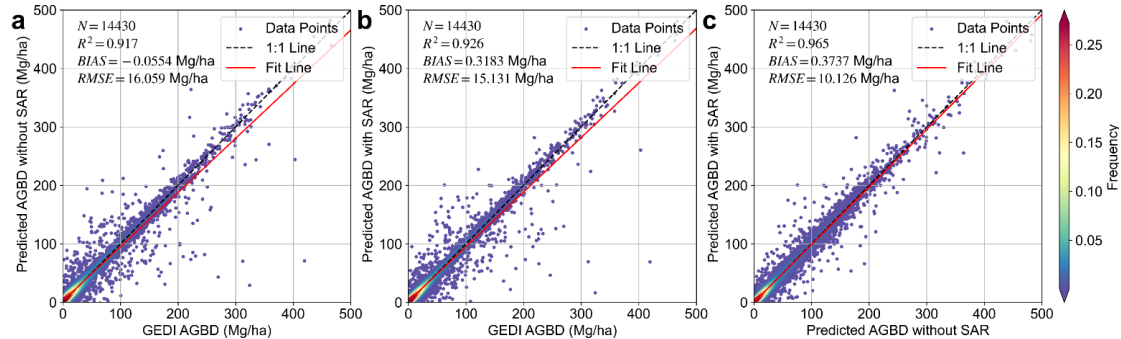
Text Fig. S2 | Comparison of AGBD estimation accuracy with and without SAR integration.

(a) Scatter plot of GEDI AGBD vs. predicted AGBD without SAR. (b) Scatter plot of GEDI AGBD vs. predicted AGBD with SAR. (c) Scatter plot comparing predicted AGBD with SAR integration to predicted AGBD without SAR.

Text Table 4. Estimation accuracy using different feature combinations along AGBD intervals.

Intervals of AGBD (Mg/ha)	Feature combinations	RMSE (Mg/ha)	Bias (Mg/ha)

[0, 50)	With SAR	6.40	0.62
	Without SAR	7.79	1.26
[50, 100)	With SAR	18.25	-0.24
	Without SAR	17.41	-0.34
[100, 150)	With SAR	19.51	-2.24
	Without SAR	20.35	-2.94
[150, 200)	With SAR	24.41	-4.82
	Without SAR	28.56	-6.91
≥200	With SAR	75.50	-24.37
	Without SAR	78.17	-24.63

Supplementary Table (1–2)

Table S1. The average forest AGBD and total carbon stock in China from difference AGB datasets.

Temporal coverage	Average forest AGBD (Mg/ha)	Total forest carbon stock (PgC)	Sources
2004	160.74 ± 45.16	8.20	Hu et al., (2016)
2004	121.93	9.06	Su et al., (2016)
2006	69.88	5.44	Huang et al., (2019)
2010	57.05	5.04	Santoro et al., (2021)
2009–2013	89.04	7.27	Zhao et al., (2019)
2011–2015 (Optimal weighting technique)	92.29±21.14	7.73	Chang et al., (2021)
2011–2015 (Random forest regression)	96.64±28.43	8.13	
2018	89.2	8.32	Tang et al., (2018)
2018	95.4	9.35	Xu et al., (2018)
2019	97.57±23.85	11.06	Yang et al., (2023)

Table S2. Sample Distribution Across Ecoregions for RseNet Model training and testing.

| Ecoregions	Training sample size	Testing samples size	Sample size	Area (10^4 km²)	Sample density (Samples per 10^4 km²)
Temperate desert	25524	6385	31909	334.5	95.4
Tibetan plateau alpine vegetation	11239	2882	14121	160.6	87.9
Subtropical evergreen broadleaf forest	10647	2610	13257	267.0	49.6
Tropical monsoon rainforest and rainforest	1154	294	1448	29.0	49.9
Warm temperate deciduous broadleaf forest	6114	1521	7635	97.1	78.6
Temperate coniferous and deciduous broadleaf mixed forest	2118	497	2615	40.8	64.1
Cold temperate coniferous forest	934	241	1175	20.9	56.2
Total	57720	14430	72160	949.9	76.0

Supplementary Figure (1–4)
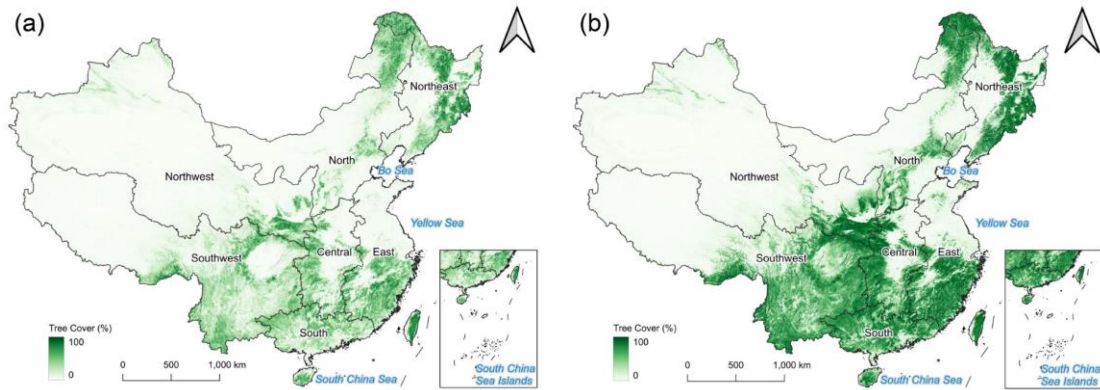
Fig. S1. Tree cover change in China between 1985 and 2023. (a) and (b) are the spatial distribution of tree cover in China for the years 1985 and 2023, respectively. Tree cover data sources from CATCD (Cai et al., 2024).
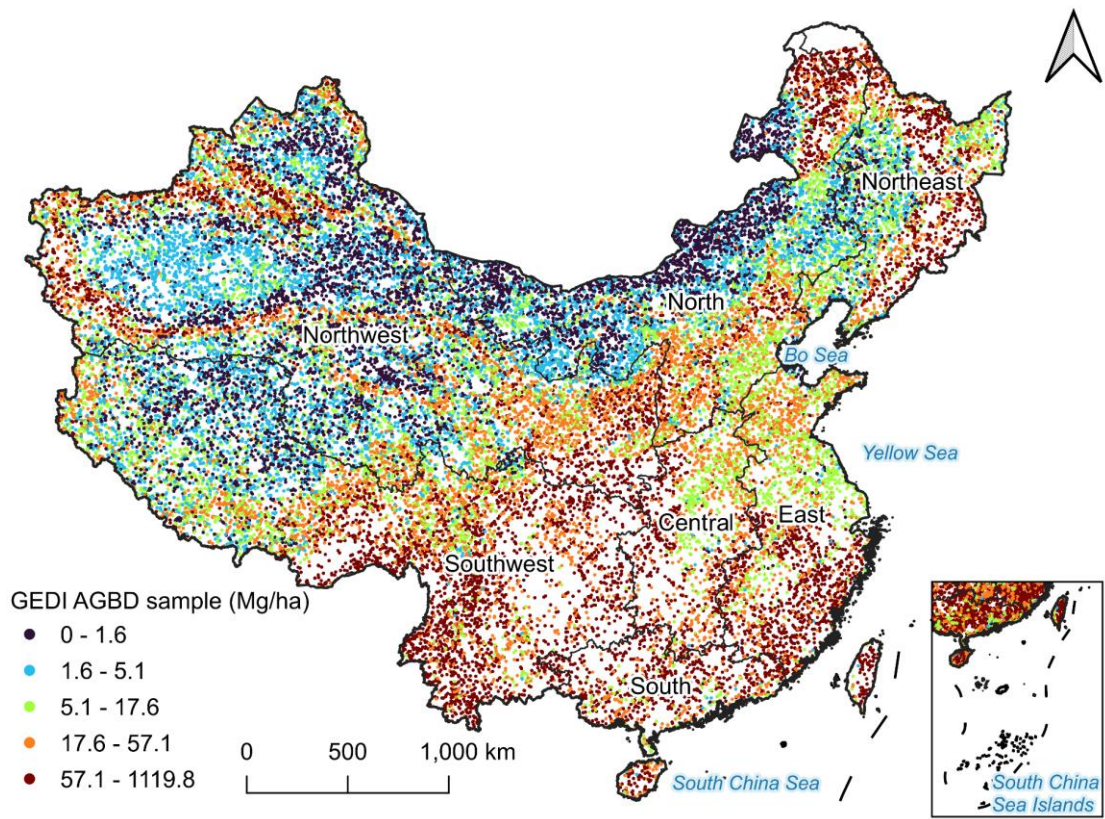
Fig. S2. Spatial distribution of GEDI AGBD samples between 2019 to 2021 within China.
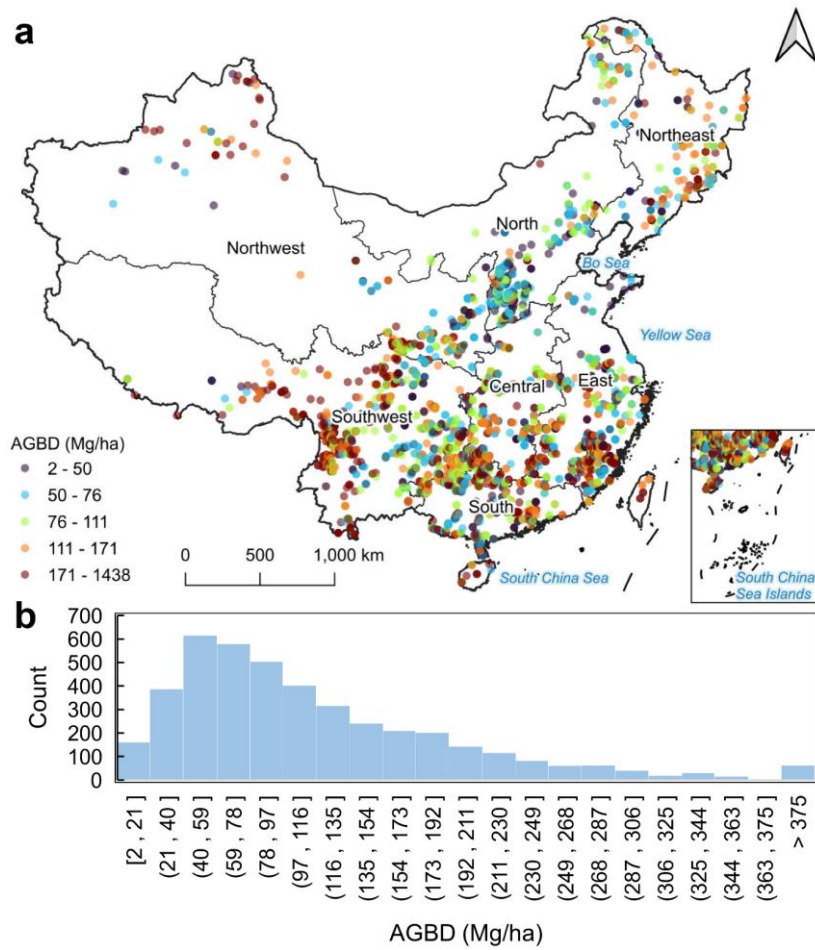
Fig. S3. Overview of field survey data across China from the 1990s to the 2010s. (a) Spatial distribution of field survey sites. (b) Frequency distribution of field survey data by AGBD interval.
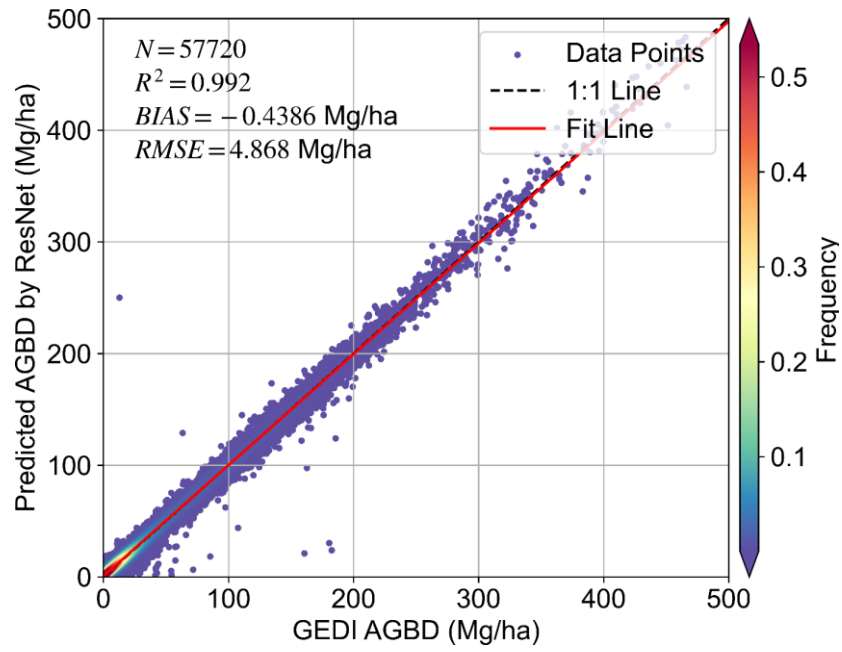
Fig. S4. Scatter plot of GEDI AGBD (training set) vs. ResNet estimated AGBD.

Bibliography

Breiman, L. (2001). Random Forests. Machine Learning, 45(1), 5–32. https://doi.org/10.1023/A:1010933404324

Cai, Y., Xu, X., Zhu, P., Nie, S., Wang, C., Xiong, Y., and Liu, X.: Unveiling spatiotemporal tree cover patterns in China: The first 30 m annual tree cover mapping from 1985 to 2023, ISPRS J. Photogramm. Remote Sens., https://doi.org/10.1016/j.isprsjprs.2024.08.001, 2024.

Chang, Z., Hobeichi, S., Wang, Y.-P., Tang, X., Abramowitz, G., Chen, Y., Cao, N., Yu, M., Huang, H., Zhou, G., Wang, G., Ma, K., Du, S., Li, S., Han, S., Ma, Y., Wigneron, J.-P., Fan, L., Saatchi, S. S., and Yan, J.: New Forest Aboveground Biomass Maps of China Integrating Multiple Datasets, Remote Sens., 13, 2892, https://doi.org/10.3390/rs13152892, 2021.

Chen, T., & Guestrin, C. (2016). XGBoost: A Scalable Tree Boosting System. Proceedings of the 22nd ACM SIGKDD International Conference on Knowledge Discovery and Data Mining, 785–794. https://doi.org/10.1145/2939672.2939785

Chen, Y., Feng, X., Fu, B., Ma, H., Zohner, C. M., Crowther, T. W., Huang, Y., Wu, X., and Wei, F.: Maps with 1 km resolution reveal increases in above- and belowground forest biomass carbon pools in China over the past 20 years, Earth Syst. Sci. Data, 15, 897–910, https://doi.org/10/gsdz4p, 2023.

Fang, H., Fan, L., Ciais, P., Xiao, J., Fensholt, R., Chen, J., Frappart, F., Ju, W., Niu, S., Xiao, X., Yuan, W., Xia, J., Li, X., Liu, L., Qin, Y., Chang, Z., Yu, L., Dong, G., Cui, T., Li, X., and Wigneron, J.-P.: Satellite-based monitoring of China's above-ground biomass carbon sink from 2015 to 2021, Agric. For. Meteorol., 356, 110172, https://doi.org/10.1016/j.agrformet.2024.110172, 2024.

Harris, N. L., Gibbs, D. A., Baccini, A., Birdsey, R. A., De Bruin, S., Farina, M., Fatoyinbo, L., Hansen, M. C., Herold, M., Houghton, R. A., Potapov, P. V., Suarez, D. R., Roman-Cuesta, R. M., Saatchi, S. S., Slay, C. M., Turubanova, S. A., and Tyukavina, A.: Global maps of twenty-first century forest carbon fluxes, Nat. Clim. Change, 11, 234–240, https://doi.org/10.1038/s41558-020-00976-6, 2021.

He, H., Wang, S., Zhang, L., Wang, J., Ren, X., Zhou, L., Piao, S., Yan, H., Ju, W., Gu, F., Yu, S.,

Yang, Y., Wang, M., Niu, Z., Ge, R., Yan, H., Huang, M., Zhou, G., Bai, Y., Xie, Z., Tang, Z., Wu, B., Zhang, L., He, N., Wang, Q., and Yu, G.: Altered trends in carbon uptake in China's terrestrial ecosystems under the enhanced summer monsoon and warming hiatus, Natl. Sci. Rev., 6, 505–514, https://doi.org/10.1093/nsr/nwz021, 2019.

HENGEVELD, G. M., GUNIA, K., DIDION, M., ZUDIN, S., CLERKX, A. P. P. M., and SCHELHAAS, M. J.: Global 1-degree Maps of Forest Area, Carbon Stocks, and Biomass, 1950-2010, https://doi.org/10.3334/ORNLDAAC/1296, 2015.

Hu, T., Su, Y., Xue, B., Liu, J., Zhao, X., Fang, J., and Guo, Q.: Mapping Global Forest Aboveground Biomass with Spaceborne LiDAR, Optical Imagery, and Forest Inventory Data, Remote Sens., 8, 565, https://doi.org/10.3390/rs8070565, 2016.

Huang, H., Liu, C., Wang, X., Zhou, X., and Gong, P.: Integration of multi-resource remotely sensed data and allometric models for forest aboveground biomass estimation in China, Remote Sens. Environ., 221, 225–234, https://doi.org/10.1016/j.rse.2018.11.017, 2019.

Ke, G., Meng, Q., Finley, T., et al. (2017). LightGBM: A Highly Efficient Gradient Boosting Decision Tree. Advances in Neural Information Processing Systems, 30.

Liu, Y. Y., Van Dijk, A. I. J. M., De Jeu, R. A. M., Canadell, J. G., McCabe, M. F., Evans, J. P., and Wang, G.: Recent reversal in loss of global terrestrial biomass, Nat. Clim. Change, 5, 470–474, https://doi.org/10.1038/nclimate2581, 2015.

Pan, Y., Birdsey, R. A., Fang, J., Houghton, R., Kauppi, P. E., Kurz, W. A., Phillips, O. L., Shvidenko, A., Lewis, S. L., Canadell, J. G., Ciais, P., Jackson, R. B., Pacala, S. W., McGuire, A. D., Piao, S., Rautiainen, A., Sitch, S., and Hayes, D.: A Large and Persistent Carbon Sink in the World's Forests, Science, 333, 988–993, https://doi.org/10.1126/science.1201609, 2011.

Piao, S., Fang, J., Ciais, P., Peylin, P., Huang, Y., Sitch, S., and Wang, T.: The carbon balance of terrestrial ecosystems in China, Nature, 458, 1009–1013, https://doi.org/10.1038/nature07944, 2009.

Santoro, M., Cartus, O., Carvalhais, N., Rozendaal, D. M. A., Avitabile, V., Araza, A., de Bruin, S.,

Herold, M., Quegan, S., Rodríguez-Veiga, P., Balzter, H., Carreiras, J., Schepaschenko, D., Korets, M., Shimada, M., Itoh, T., Moreno Martínez, Á., Cavlovic, J., Cazzolla Gatti, R., da Conceição Bispo, P., Dewnath, N., Labrière, N., Liang, J., Lindsell, J., Mitchard, E. T. A., Morel, A., Pacheco Pascagaza, A. M., Ryan, C. M., Slik, F., Vaglio Laurin, G., Verbeeck, H., Wijaya, A., and Willcock, S.: The global forest above-ground biomass pool for 2010 estimated from high-resolution satellite observations, Earth Syst. Sci. Data, 13, 3927–3950, https://doi.org/10.5194/essd-13-3927-2021, 2021.

Su, Y., Guo, Q., Xue, B., Hu, T., Alvarez, O., Tao, S., and Fang, J.: Spatial distribution of forest aboveground biomass in China: Estimation through combination of spaceborne lidar, optical imagery, and forest inventory data, Remote Sens. Environ., 173, 187–199, https://doi.org/10.1016/j.rse.2015.12.002, 2016.

Tang, X., Zhao, X., Bai, Y., Tang, Z., Wang, W., Zhao, Y., Wan, H., Xie, Z., Shi, X., Wu, B., Wang, G., Yan, J., Ma, K., Du, S., Li, S., Han, S., Ma, Y., Hu, H., He, N., Yang, Y., Han, W., He, H., Yu, G., Fang, J., and Zhou, G.: Carbon pools in China's terrestrial ecosystems: New estimates based on an intensive field survey, Proc. Natl. Acad. Sci., 115, 4021–4026, https://doi.org/10.1073/pnas.1700291115, 2018.

Wang, J., Feng, L., Palmer, P. I., Liu, Y., Fang, S., Bösch, H., O'Dell, C. W., Tang, X., Yang, D., Liu, L., and Xia, C.: Large Chinese land carbon sink estimated from atmospheric carbon dioxide data, Nature, 586, 720–723, https://doi.org/10.1038/s41586-020-2849-9, 2020.

Xia, X., Xia, J., Chen, X., Fan, L., Liu, S., Qin, Y., Qin, Z., Xiao, X., Xu, W., Yue, C., Yue, X., and Yuan, W.: Reconstructing Long-Term Forest Cover in China by Fusing National Forest Inventory and 20 Land Use and Land Cover Data Sets, J. Geophys. Res. Biogeosciences, 128, e2022JG007101, https://doi.org/10.1029/2022JG007101, 2023.

Xu, L., Yu, G., He, N., Wang, Q., Gao, Y., Wen, D., Li, S., Niu, S., and Ge, J.: Carbon storage in China's terrestrial ecosystems: A synthesis, Sci. Rep., 8, 2806, https://doi.org/10.1038/s41598-018-20764-9, 2018.

Yang, Q., Niu, C., Liu, X., Feng, Y., Ma, Q., Wang, X., Tang, H., and Guo, Q.: Mapping high-resolution forest aboveground biomass of China using multisource remote sensing data, GIScience Remote Sens., 60, 2203303, https://doi.org/10.1080/15481603.2023.2203303, 2023.

Yin, G., Zhang, Y., Sun, Y., Wang, T., Zeng, Z., and Piao, S.: MODIS Based Estimation of Forest Aboveground Biomass in China, PLOS ONE, 10, e0130143, https://doi.org/10.1371/journal.pone.0130143, 2015.

Yu, Z., Ciais, P., Piao, S., Houghton, R. A., Lu, C., Tian, H., Agathokleous, E., Kattel, G. R., Sitch, S., Goll, D., Yue, X., Walker, A., Friedlingstein, P., Jain, A. K., Liu, S., and Zhou, G.: Forest expansion dominates China's land carbon sink since 1980, Nat. Commun., 13, 5374, https://doi.org/10.1038/s41467-022-32961-2, 2022.

Zarin, D. J., Harris, N. L., Baccini, A., Aksenov, D., Hansen, M. C., Azevedo-Ramos, C., Azevedo, T., Margono, B. A., Alencar, A. C., Gabris, C., Allegretti, A., Potapov, P., Farina, M., Walker, W. S., Shevade, V. S., Loboda, T. V., Turubanova, S., and Tyukavina, A.: Can carbon emissions from tropical deforestation drop by 50% in 5 years?, Glob. Change Biol., 22, 1336–1347, https://doi.org/10.1111/gcb.13153, 2016.

Zhao, M., Yang, J., Zhao, N., Liu, Y., Wang, Y., Wilson, J. P., and Yue, T.: Estimation of China's forest stand biomass carbon sequestration based on the continuous biomass expansion factor model and seven forest inventories from 1977 to 2013, For. Ecol. Manag., 448, 528–534, https://doi.org/10.1016/j.foreco.2019.06.036, 2019.

Zhao, M., Yang, J., Zhao, N., Liu, L., Du, L., Xiao, X., Yue, T., and Wilson, J. P.: Spatially explicit changes in forest biomass carbon of China over the past 4 decades: Coupling long-term inventory and remote sensing data, J. Clean. Prod., 316, 128274, https://doi.org/10.1016/j.jclepro.2021.128274, 2021.

Ke, G., Meng, Q., Finley, T., Wang, T., Chen, W., Ma, W., ... & Liu, T. Y. (2017). Lightgbm: A highly efficient gradient boosting decision tree. *Advances in neural information processing systems*, *30*.

Chen, T., & Guestrin, C. (2016, August). Xgboost: A scalable tree boosting system. In *Proceedings of the 22nd acm sigkdd international conference on knowledge discovery and data mining* (pp. 785-794).